

Numerical evaluation of multi-loop integrals by sector decomposition

T. Binoth^a and G. Heinrich^b

^a*School of Physics, The University of Edinburgh,
EH9 3JZ Edinburgh, Scotland, UK*

^b*IPPP, University of Durham, Durham DH1 3LE, UK*

Abstract

In a recent paper [1] we have presented an automated subtraction method for divergent multi-loop/leg integrals in dimensional regularisation which allows for their numerical evaluation, and applied it to diagrams with massless internal lines. Here we show how to extend this algorithm to Feynman diagrams with massive propagators and arbitrary propagator powers. As applications, we present numerical results for the master 2-loop 4-point topologies with massive internal lines occurring in Bhabha scattering at two loops, and for the master integrals of planar and non-planar massless double box graphs with two off-shell legs. We also evaluate numerically some two-point functions up to 5 loops relevant for beta-function calculations, and a 3-loop 4-point function, the massless on-shell planar triple box. Whereas the 4-point functions are evaluated in non-physical kinematic regions, the results for the propagator functions are valid for arbitrary kinematics.

1 Introduction

The precision of present and upcoming high energy experiments is unprecedented and clearly requires an analogous level of accuracy on the theoretical side. One of the steps towards achieving this goal is to push the level of higher order corrections in perturbation theory further. However, the calculation of the corresponding Feynman diagrams becomes more and more involved as the number of loops and legs of the graphs increases. Typically the occurring tensor integrals are expressed in terms of scalar integrals which are then reduced to a set of master topologies. These master topologies are the basic ingredients and thus the bottleneck for any attempt to perform a higher order calculation.

A milestone in this respect has been the analytic calculation of the master integrals for the planar [2] and non-planar [3] massless two-loop box diagrams with on-shell external legs and the ones with one external leg off-shell [4, 5, 6, 7]. These results triggered the analytical computation of two-loop matrix elements for $2 \rightarrow 2$ scattering processes with on-shell legs [8] and $1 \rightarrow 3$ processes with one off-shell leg [9], which are necessary for the next-to-next-to-leading order calculation of prominent processes like two-jet production in hadronic collisions or three-jet production in e^+e^- collisions. On the other hand, the two-loop four-point functions with two external legs off-shell still await their analytical calculation. These integrals are for example needed to calculate the production of two massive vector bosons in hadronic collisions at two loops.

The reason for the lack of analytical results is the increasing number of scales as the number of off-shell legs increases, leading to more complicated analytic structures. The same argument is true if the diagrams contain massive internal lines. Such diagrams are certainly important in view of a forthcoming e^+e^- collider at TeV energies, where the experimental precision will be such that the Standard Model is tested at the two-loop level. However, a major part of the corresponding two-loop master integrals with massive propagators may not be accessible analytically. Thus the development of numerical methods seems natural to make progress in loop calculations.

This is not at all straightforward, as different kinds of singularities – infrared (IR), ultraviolet (UV) and threshold singularities – are present. Even in the absence of IR and UV divergences, one has to face problems due to a complicated analytic structure: For physical kinematics the integral generically has singularities within the integration region, which typically hinder a successful, numerically stable evaluation. At the one-loop level this problem is less severe because the integration space can be reduced to lower dimensionality and because the analytical structure is completely understood. Solutions for multi-leg one-loop diagrams have been suggested in [10, 11]. However, beyond one loop the problem is not satisfactorily solved in a general and constructive way, although promising approaches have been proposed [12, 13, 14, 15]. In the presence of infrared divergences the situation is even more difficult. One first has to obtain a numerically integrable function by subtracting the infrared poles. As

these poles are in general overlapping, this is a highly non-trivial task. In this paper we will focus on this problem, i.e. on the isolation of infrared divergences from general multi-loop Feynman diagrams.

In [1] we proposed a constructive method which enables to calculate multi-loop integrals numerically for unphysical kinematics, and applied it to diagrams with massless propagators. It served to check the results for the massless on-shell double boxes and to make predictions for the massless double boxes with one off-shell leg, the latter being confirmed by the subsequent analytical calculation later. This method is based on *sector decomposition*, originally used to disentangle overlapping UV divergences in the proof of the BPHZ theorem [16]. The basic concept being very simple, it has a wide range of applicability. For example, it has been used to derive high energy approximations for one-loop integrals [17]. Sector decomposition also has been employed to extract logarithmic mass singularities from massive multi-scale integrals in the high energy limit at two loops [18]. In [1], the concept of sector decomposition has been elaborated to a highly automated program package, allowing to convert dimensionally regulated Feynman integrals into a Laurent series in ϵ . The coefficients of the poles are sums of multi-dimensional parameter integrals. In a kinematic region where thresholds are absent, the latter can be evaluated with standard numerical integration routines. In simple cases, analytic integration is also possible. The numbers of loops and legs are in principle arbitrary, but of course limited by CPU time and disk space. Recently the method has been extended to deal also with phase space integrals [19].

In this article, we show how to generalise the proposed method to arbitrary Feynman diagrams. This is achieved by extending the algorithm to graphs with arbitrary masses and propagator exponents. With these extensions one is able to deal with very different types of multi-loop/multi-scale problems, most of which are at the edge or beyond the present state of the art of analytic calculations. More precisely, we present numerical results for massless two-loop 4-point functions with two external legs off-shell, and for the three most difficult master topologies for Bhabha scattering at two loops, at two numerical points where $s, t < 0$. We also give numerical results for 3-loop, 4-loop and 5-loop massless 2-point functions relevant for the calculation of beta-functions, and finally for the massless on-shell planar 3-loop box diagram. Although we do not provide a solution for arbitrary physical kinematics in general, we note that there is an important class of diagrams, namely diagrams with only one scale, where there is no kinematical restriction.

The paper is organised as follows. In section 2, we briefly present the method, extended to include also non-integer propagator powers, respectively Feynman parameters in the numerator. In section 3 we collect applications of the method, presenting numerical results for the types of diagrams listed above. Section 4 contains the discussion of our results and the conclusions.

2 The formalism

The formalism of iterated sector decomposition enables to extract in a constructive way the divergences of arbitrary scalar L -loop N -point integrals, where the divergences are regularised by dimensional regularisation. The method has been described in detail in [1]. Here we only sketch it briefly, focusing on the features that have not been elaborated previously, i.e. the possibility of arbitrary propagator powers and the inclusion of massive propagators.

A scalar graph G with N propagators and L D -dimensional loop momenta, where the propagators can have arbitrary, not necessarily integer powers ν_j , has the following representation in momentum and Feynman parameter space¹:

$$\begin{aligned} G &= \int \prod_{l=1}^L \frac{d^D k_l}{i\pi^{\frac{D}{2}}} \prod_{j=1}^N \frac{1}{(q_j^2 - m_j^2 + i\delta)^{\nu_j}} \\ &= (-1)^{N_\nu} \frac{\Gamma(N_\nu - LD/2)}{\prod_{j=1}^N \Gamma(\nu_j)} \int_0^\infty \prod_{j=1}^N dx_j x_j^{\nu_j-1} \delta(1 - \sum_{i=1}^N x_i) \frac{\mathcal{U}^{N_\nu - (L+1)D/2}}{\mathcal{F}^{N_\nu - LD/2}} \end{aligned} \quad (1)$$

Here q_j are the propagator momenta, i.e. linear combinations of external and loop momenta, $N_\nu = \sum_{j=1}^N \nu_j$. The functions \mathcal{U} and \mathcal{F} can be straightforwardly derived from the momentum representation. They also can be constructed from the topology of the corresponding Feynman graph as follows.

Cutting L lines of a given connected L -loop graph such that it becomes a connected tree graph T defines a *chord* $\mathcal{C}(T)$ as being the set of lines not belonging to this tree. The Feynman parameters associated with each chord define a monomial of degree L . The set of all such trees (or *1-trees*) is denoted by \mathcal{T}_1 . The 1-trees $T \in \mathcal{T}_1$ define \mathcal{U} as being the sum over all monomials corresponding to a chord $\mathcal{C}(T \in \mathcal{T}_1)$. Cutting one more line of a 1-tree leads to two disconnected trees, or a *2-tree* \hat{T} . \mathcal{T}_2 is the set of all such 2-trees. The corresponding chords define monomials of degree $L + 1$. Each 2-tree of a graph corresponds to a cut defined by cutting the lines which connected the 2 now disconnected trees in the original graph. The momentum flow through the lines of such a cut defines a Lorentz invariant $s_{\hat{T}} = (\sum_{j \in \text{Cut}(\hat{T})} p_j)^2$. The function \mathcal{F}_0 is the sum over all such monomials times minus the corresponding invariant:

$$\begin{aligned} \mathcal{U}(\vec{x}) &= \sum_{T \in \mathcal{T}_1} \left[\prod_{j \in \mathcal{C}(T)} x_j \right], \\ \mathcal{F}_0(\vec{x}) &= \sum_{\hat{T} \in \mathcal{T}_2} \left[\prod_{j \in \mathcal{C}(\hat{T})} x_j \right] (-s_{\hat{T}}), \\ \mathcal{F}(\vec{x}) &= \mathcal{F}_0(\vec{x}) + \mathcal{U}(\vec{x}) \sum_{j=1}^N x_j m_j^2. \end{aligned} \quad (2)$$

¹This representation, as well as the following discussion of its topological properties, is well known, see for example [22, 23, 24, 26, 15].

\mathcal{U} is a positive semi-definite function. Its vanishing is related to the UV subdivergences of the graph. Overall UV divergences, if present, will always be contained in the prefactor $\Gamma(N_\nu - LD/2)$. In the Euclidean region, \mathcal{F} is also a positive semi-definite function of the Feynman parameters x_j . Its vanishing does not necessarily lead to an IR singularity. Only if some of the invariants are zero, for example if some of the external momenta are light-like, the vanishing of \mathcal{F} may induce an IR divergence. Thus it depends on the *kinematics* and not only on the topology (like in the UV case) whether a zero of \mathcal{F} leads to a divergence or not. This fact makes it much harder to formulate general theorems on the IR singularity structure of Feynman graphs. Examples of \mathcal{U} and \mathcal{F} functions will be given below.

In multi-loop integrals, the singular regions – leading to at most $1/\epsilon^{2L}$ infrared poles upon integration in parameter space – are generally *overlapping*, such that the set-up of a simple subtraction scheme becomes impossible. In [1] we have developed an algorithm and computer program to disentangle such overlapping regions. It can briefly be sketched as follows:

Step 1: A "primary" sector decomposition of all Feynman parameters eliminates the δ -function and maps the integral to a sum of N $(N-1)$ -dimensional parameter integrals over the unit cube: The decomposition

$$\int d^N x = \sum_{l=1}^N \int d^N x \prod_{\substack{j=1 \\ j \neq l}}^N \theta(x_l \geq x_j \geq 0)$$

and appropriate variable substitutions lead to

$$G = \sum_{l=1}^N G_l, \quad G_l = \int_0^1 \prod_{i=1}^{N-1} dx_i \frac{\mathcal{U}_l^{N-(L+1)D/2}(\vec{x})}{\mathcal{F}_l^{N-LD/2}(\vec{x})},$$

where $\mathcal{U}_l, \mathcal{F}_l$ contain only positive semi-definite functions and where the singularities can only be located at $x_i = 0$.

Step 2: Sector decomposition is performed iteratively for sets of parameters $\{x_k\}$ which make the transformed $\hat{\mathcal{F}}$ or $\hat{\mathcal{U}}$ functions vanish at $x_k = 0$. The iteration stops if $\hat{\mathcal{U}} = 1 + \dots$ and $\hat{\mathcal{F}} = (-s_{ij}) + \dots$, where the dots denote positive semi-definite remainder terms and $(-s_{ij})$ is a kinematic invariant which is assumed to be positive. At this point all divergences are non-overlapping, the poles will be entirely contained in overall factors $x_i^{\alpha+\beta\epsilon}$, with α a negative integer.

Step 3: Subtractions are performed using Taylor expansion around $x_i = 0$. After subtraction, it is safe to expand in ϵ up to the desired order, leading to the form

$$G = \sum_{j=-M}^{2L} \frac{C_j(\vec{x})}{\epsilon^j} + O(\epsilon^{M+1}). \quad (3)$$

Note that the method in principle allows to calculate coefficients of the Laurent series in ϵ to arbitrary order M .

Step 4: The coefficients $C_m(\vec{x})$ in (3) are sums of subtracted and expanded subsector integrals in terms of bounded functions of Feynman parameters. These can be evaluated numerically, or even analytically in simple cases.

In [1] we were concentrating on massless integrals. The iteration always stopped, as each sector decomposition reduces the degree of the monomials which are relevant for the IR behaviour of the integral. Including propagator masses, it is clear that the IR behaviour of a diagram can only improve, and hence this extension of the algorithm does not pose any principle problem. On the other hand, a new technical feature appears, which is that the Feynman parameters associated with massive lines occur quadratically in \mathcal{F} , stemming from the term proportional to \mathcal{U} in eq. (2). In this case it is not guaranteed that the iteration stops if one proceeds thoughtlessly. For example, it is easy to see that a polynomial of the type $xy^2 + z^2$ can produce an endless loop if a sector decomposition in $\{x, z\}$ is followed by one in $\{x, y\}$. A possible way out is to decompose first all parameters which occur quadratically, in our example $\{y, z\}$. Then no dangerous situation is present anymore and one can proceed as usual. The corresponding modification of the code is straightforward, and examples of such a situation are the two-loop QED graphs calculated below.

We note that with the generalisation of the algorithm presented in this article, integrals with arbitrary numerators, and thus tensor integrals, can be treated. As is well known, after integration over the loop momenta, tensor integrals correspond to linear combinations of integrals with monomials of Feynman parameters in the numerator (times tensors carrying the Lorentz structure). These numerators are taken into account by our program and may cancel IR singularities which would be present in the scalar diagram. Another possibility is to express tensor integrals by Feynman parameter integrals which do not have polynomial numerators, but are partly in shifted dimensions, as advocated in [25, 26]. As our method treats the space-time dimension as a parameter, this way is viable as well.

3 Applications

In this section we discuss a number of applications of our algorithm, ranging from 2-loop 4-point functions to 5-loop 2-point functions. We note that sector decomposition also is useful for the calculation of graphs which are not plagued by IR or UV divergences, as it produces integrands which are bounded and positive definite in kinematic regions where no thresholds are approached. The technical problem of integrable singularities inside multi-dimensional integration regions hinders the direct computation of the parameter integrals for general kinematics. However, this is not a limitation intrinsic to our procedure, as more sophisticated numerical integration

routines than the one we use could overcome this problem. However, for the time being, we have to restrict ourselves to the non-physical region, where all Mandelstam variables are negative, in the case of the box functions.

For the numerical evaluations we have used the standard Monte Carlo package BASES [30]. The numerical precision for all quoted results is 1% or better.

The integration time for all 2-loop boxes to reach the demanded precision is of the order of an hour on a PC with a Pentium IV (2 GHz) processor. For the 3-loop propagators the required time is less, whereas for the 5-loop propagator it took a few days to reach this precision.

3.1 Parameter representation of general double box graphs

As the topological functions \mathcal{U} and \mathcal{F} are the basic input for our algorithm, we first give the parameter representation of the general planar and non-planar double box topologies. These representations are used as a starting point for the particular 2-loop box examples calculated below.

Planar topology

The functions \mathcal{U} and \mathcal{F} for the planar double box graph $G_P(s, t, u, s_1, s_2, s_3, s_4, \{m_j^2\})$, as shown in Fig. (1a), are given by

$$\begin{aligned}
\mathcal{U} &= x_{123}x_{567} + x_4x_{123567} \\
\mathcal{F} &= (-s)(x_2x_3x_{4567} + x_5x_6x_{1234} + x_2x_4x_6 + x_3x_4x_5) + (-t)x_1x_4x_7 \\
&\quad + (-s_1)x_1(x_4x_5 + x_2x_{4567}) + (-s_2)x_1(x_4x_6 + x_3x_{4567}) \\
&\quad + (-s_3)x_7(x_3x_4 + x_6x_{1234}) + (-s_4)x_7(x_2x_4 + x_5x_{1234}) \\
&\quad + \mathcal{U} \sum_{j=1}^7 x_j m_j^2
\end{aligned} \tag{4}$$

where we use the short-hand notations $s_i = p_i^2$, $s = (p_1 + p_2)^2$, $t = (p_2 + p_3)^2$ and $x_{i_1\dots i_n} = x_{i_1} + \dots + x_{i_n}$. In the examples considered in the following, we will set some of the s_i and/or m_j^2 to zero.

Non-planar topology

The parameter representation of the general non-planar double box $G_{NP}(s, t, u, s_1, s_2, s_3, s_4, \{m_j^2\})$, Fig. (1b), is given by

$$\begin{aligned}
\mathcal{U} &= x_{123}x_{4567} + x_{45}x_{67} \\
\mathcal{F} &= (-s)(x_2x_3x_{4567} + x_2x_4x_6 + x_3x_5x_7) \\
&\quad + (-t)x_1x_4x_7 + (-u)x_1x_5x_6
\end{aligned}$$

$$\begin{aligned}
& + (-s_1) x_1 (x_5 x_7 + x_2 x_{4567}) + (-s_2) x_1 (x_4 x_6 + x_3 x_{4567}) \\
& + (-s_3) (x_6 x_7 x_{12345} + x_3 x_4 x_7 + x_2 x_5 x_6) \\
& + (-s_4) (x_4 x_5 x_{12367} + x_3 x_5 x_6 + x_2 x_4 x_7) \\
& + \mathcal{U} \sum_{j=1}^7 x_j m_j^2 .
\end{aligned} \tag{5}$$

3.2 Massless double box graphs with two legs off-shell

For the massless 4-point functions considered in this subsection, two legs are off-shell and the internal lines are massless. The topologically different positions of the off-shell legs give rise to three master integrals for both the planar- and the non-planar double box with two legs off-shell. We give results at two Euclidean numerical points for each master integral, as shown in Tables 1 and 2. An overall factor $\Gamma^2(1 + \epsilon)$ has been extracted:

$$G_{\text{P, NP}}(s, t, u, s_1, s_2, s_3, s_4) = \Gamma^2(1 + \epsilon) \sum_{i=0}^4 \frac{P_i}{\epsilon^i}$$

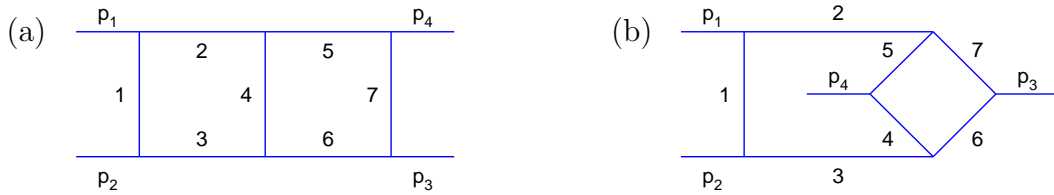


Figure 1: *The (a) planar and (b) non-planar double box.*

We would like to note at this point that our method is not a priori a numerical method. In principle, the functions obtained after step 3 of the algorithm can be integrated analytically. However, as the parameter integrals for the coefficient of the $1/\epsilon^l$ pole are $(N - 1 - l)$ -dimensional, and the functions to integrate are in general highly non-trivial, only the integrals for large l , i.e. the highest pole coefficients, can be evaluated automatically by standard algebraic integration packages. For example, one obtains the following analytical result for the leading and subleading poles of the planar topology with $s_3 \neq 0, s_4 \neq 0$:

$$\begin{aligned}
G_{\text{P}}(s, t, u, 0, 0, s_3, s_4) &= \Gamma^2(1 + \epsilon) (-s)^{-2\epsilon} \frac{1}{s^2 t} \left\{ \frac{1}{4\epsilon^4} \right. \\
&\quad \left. + \frac{1}{\epsilon^3} \left[-\log(-t) + \frac{1}{2} \log(-s_3) + \frac{1}{2} \log(-s_4) \right] \right\} + \mathcal{O}\left(\frac{1}{\epsilon^2}\right)
\end{aligned}$$

Although the analytic integration could be pushed further by writing algebraic integration routines which are specialised to deal with the functions occurring in these integrals, we do not pursue the analytic approach further here.

$(-s, -t, -u) = (2/3, 2/3, 2/3)$			
$(-s_1, -s_2, -s_3, -s_4)$	$(1, 0, 0, 1)$	$(0, 1, 0, 1)$	$(0, 0, 1, 1)$
P_4	-0.8437	0	-0.8438
P_3	-2.052	0	-2.053
P_2	-2.189	-3.571	-10.53
P_1	4.394	-6.585	-48.60
P_0	35.64	11.83	-140.7

$(-s, -t, -u) = (1/2, 1/3, 5/6)$			
$(-s_1, -s_2, -s_3, -s_4)$	$(2/3, 0, 0, 1)$	$(0, 2/3, 0, 1)$	$(0, 0, 2/3, 1)$
P_4	-3.000	0	-3.000
P_3	-12.47	0	-14.91
P_2	-26.28	-7.827	-73.79
P_1	-19.04	-18.90	-325.3
P_0	90.68	16.18	-1151.

Table 1: Numerical results for the planar double box with two off-shell legs

3.3 Double Box graphs for Bhabha scattering

Bhabha scattering is a paradigm process of QED. Its calculation at the two-loop level, apart from the theoretical challenge alone, has a strong motivation by the fact that Bhabha scattering serves as a luminosity monitor for e^+e^- colliders.

The virtual two-loop QED corrections to Bhabha scattering have been calculated analytically by Bern, Dixon and Ghinculov [8], in the limit of vanishing electron mass. Here we give numerical results for the three 2-loop box master integrals entering these corrections with *massive* internal lines. The numerical points are calculated for nonphysical kinematics, $s, t < 0$, but they can serve as a strong check for a future analytic calculation which includes the fermion masses.

The three master topologies $G_{l=a,b,c}$ are shown in Fig. 2. The corresponding func-

$(-s, -t, -u) = (2/3, 2/3, 2/3)$			
$(-s_1, -s_2, -s_3, -s_4)$	$(1, 1, 0, 0)$	$(0, 1, 0, 1)$	$(0, 0, 1, 1)$
P_4	-2.812	-0.5625	0
P_3	-3.192	-0.0923	2.189
P_2	29.82	5.481	1.634
P_1	139.2	35.40	-17.98
P_0	365.3	170.6	-60.33
$(-s, -t, -u) = (1/2, 1/3, 5/6)$			
$(-s_1, -s_2, -s_3, -s_4)$	$(2/3, 1, 0, 0)$	$(0, 2/3, 0, 1)$	$(0, 0, 2/3, 1)$
P_4	-6.700	-0.600	0
P_3	-15.97	1.377	4.502
P_2	38.24	11.79	5.870
P_1	305.1	57.33	-36.18
P_0	1080.	267.0	-165.5

Table 2: Numerical results for the non-planar double box with two off-shell legs

tions \mathcal{U} and \mathcal{F} are given by equation (4) for G_a and G_c and by (5) for G_b :

$$G_a(s, t, u, m^2, M^2) = G_{\text{P}}(s, t, u, m^2, M^2, M^2, m^2; 0, m^2, M^2, 0, m^2, M^2, 0)$$

$$G_b(s, t, u, m^2, M^2) = G_{\text{NP}}(s, t, u, m^2, M^2, M^2, m^2; 0, m^2, M^2, 0, m^2, M^2, 0)$$

$$G_c(s, t, u, m^2, M^2) = G_{\text{P}}(s, t, u, m^2, m^2, M^2, M^2; 0, m^2, m^2, m^2, 0, 0, M^2)$$

Results for two different numerical points are given in Table 3. An overall factor $\Gamma^2(1 + \epsilon)$ has been extracted:

$$G_{l=a,b,c}(s, t, u, m^2, M^2) = \Gamma^2(1 + \epsilon) \sum_{i=0}^2 \frac{P_i}{\epsilon^i}.$$

To be slightly more general, the second point covers the case where the two massive propagator lines flowing through the graphs have different masses.

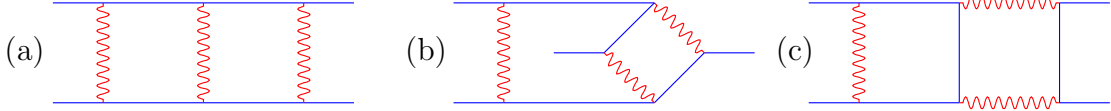


Figure 2: *The two-loop four point master topologies relevant for Bhabha scattering. The wavy lines are massless (photons) and the straight lines are massive scalars with external legs on-shell. We label the topologies from left to right by G_a , G_b , G_c .*

$(-s, -t, -u, m^2, M^2)$	$(1/5, 3/10, 7/2, 1, 1)$			$(5/3, 4/3, 5, 1, 3)$		
	G_a	G_b	G_c	G_a	G_b	G_c
P_2	-1.561	-0.5255	-1.152	-0.08622	-0.03483	-0.05832
P_1	-5.335	-0.2024	-3.690	-0.04195	0.07556	0.05389
P_0	1.421	3.606	1.555	0.7323	0.1073	0.6847

Table 3: *Results for the double box graphs for Bhabha scattering*

3.4 Propagators up to 5 loops

Due to the high complexity of multi-loop QED and QCD calculations, only a few results at the three- and four loop level are known (for a review see e.g. [28]). These results rely to a large extent on the knowledge of multi-loop propagator functions.

Massless propagator functions are very simple objects from the kinematical point of view, as they depend only on one single scale, $s = p^2$, where p is the propagator momentum. Each graph is simply given by the scale to some power times a number which can be calculated analytically or numerically once and forever.

We provide here some examples, shown in Figs. 3 to 5, to demonstrate that our method can deal with different kinds of propagator topologies up to 5 loops, and that the treatment of UV subdivergences and higher order terms in the ϵ -expansion is straightforward.

For the planar and non-planar 3-loop ladder (see Fig. 3), we get:

$$G[3a] = (-s)^{-2-3\epsilon} \Gamma(2+3\epsilon) [20.74 + 93.71 \epsilon] \quad (6)$$

$$G[3b] = (-s)^{-2-3\epsilon} \Gamma(2+3\epsilon) [20.74 + 128.4 \epsilon] \quad (7)$$

For massless internal lines, UV subdivergences appear in the form of one-loop bubble



Figure 3: 3-loop ladder-type (a) planar and (b) non-planar propagator graph.

insertions. The most convenient way to deal with them is to integrate them out analytically, which leads to a non-integer exponent of an internal propagator. An example is given in Fig. 4a:

$$G[4a] = -\frac{1}{\epsilon}(-s)^{-1-4\epsilon}\Gamma(1+4\epsilon)\text{Beta}(1-\epsilon, 1-\epsilon) [20.74 + 86.57\epsilon + 494.5\epsilon^2] \quad (8)$$

Note that in all three examples above the number $20 \cdot \zeta(5) = 20.73855\dots$ appears with the given precision². Planar 4-loop ladder, Fig. 4b:

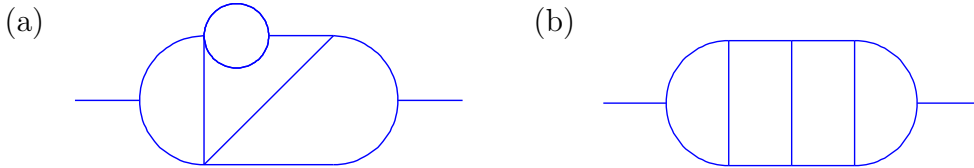


Figure 4: 4-loop propagators (a) with and (b) without UV subdivergence.

$$G[4b] = -(-s)^{-3-4\epsilon}\Gamma(3+4\epsilon) [35.10 + 197.34\epsilon] \quad (9)$$

The results for these propagator graphs agree with the analytical ones where available [27]. Finally, we also calculated a 5-loop example, shown in Fig. 5. We obtain:

$$G[5] = (-s)^{-4-5\epsilon}\Gamma(4+5\epsilon) [40.53] \quad (10)$$

3.5 Massless on-shell planar 3-loop box

In a very recent article [21] (see also [20]), Smirnov presented the analytical result for the massless on-shell planar 3-loop box $TB(s, t)$, shown in Fig. 6. We have cross-checked the analytical result by calculating a numerical value for the point $(s, t) = (-1, -3)$, and obtain

²Going to higher precision is only a question of computer time, as the integrands are positive definite and bounded.

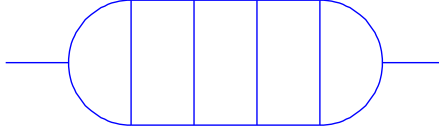


Figure 5: *A 5-loop propagator graph*

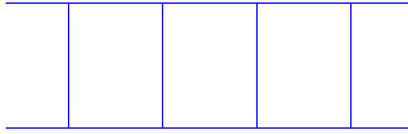


Figure 6: *Planar triple-box graph*

$$TB(-1, -3) = \Gamma(4 + 3\epsilon) \left[\frac{0.09874}{\epsilon^6} - \frac{0.7669}{\epsilon^5} - \frac{1.977}{\epsilon^4} - \frac{0.7534}{\epsilon^3} - \frac{4.747}{\epsilon^2} + \frac{2.010}{\epsilon} + 21.48 \right]$$

which is in agreement within the 1% level with the analytical result. On a PC with a 2 GHz Pentium IV processor, the full calculation took several weeks, but could have been speed up considerably by further parallelisation. However, disk space starts to become an issue here, as the size of the object files adds up to about 500 Mega Bytes.

4 Discussion and Conclusions

We have refined the formalism and automated program developed in [1] to isolate overlapping IR and UV divergences to be applicable to a very large class of Feynman graphs. The algorithm now is able to treat diagrams with arbitrary masses and propagator exponents. As discussed above, this also allows to compute Feynman integrals with non-trivial numerators. Hence we have formulated a constructive approach, based on sector decomposition, to convert dimensionally regulated Feynman diagrams into a Laurent series in ϵ , where the coefficients are given in terms of parameter integrals. These parameter integrals can always be evaluated numerically in kinematic regions where the Mandelstam variables are negative, as one can show that the integrands are bounded and positive definite in that case. As examples, we calculated numerically various 2-loop 4-point functions and a 3-loop 4-point function for

negative Mandelstam variables s, t, u . We also evaluated massless propagator graphs up to 5 loops. More precisely, we give numerical results for the following types of diagrams:

- Massless two-loop 4-point functions with two off-shell external legs (planar as well as non-planar topologies).
- The master two-loop box diagrams needed to calculate Bhabha scattering (with massive internal lines) at two loops.
- Two-point functions at 3, 4 and 5 loops, among these a 4-loop graph containing an UV subdivergence, leading to non-integer propagator powers, as well as the order ϵ terms for the 3-loop and 4-loop graphs.
- The planar 3-loop massless 4-point function with on-shell legs.

Integrals depending on a single scale, as for example massless 2-point functions, or massless 3-point functions with two on-shell legs, can be evaluated numerically if no analytical result is achievable, as they are just a number times the overall scale factor. We note that the algorithm can also be applied to vacuum graphs with UV subdivergences. In that case one has $\mathcal{F} = \mathcal{U} \sum_{j=1}^N x_j m_j^2$, and any graph can be expressed by well-behaved integrals. In this special situation other very powerful methods are known [29].

For general multi-scale problems the situation is more delicate, as for physical kinematics integrable singularities are present in a multi-dimensional integration space. The numerical integration in this case is a highly non-trivial task. For the one-loop case a combination of the sector decomposition algorithm and new numerical integration methods were proposed in [11], where it has been exploited that sector decomposition also leads to more stable integral representations if no IR/UV singularities are present. A generalisation to the two-loop case is presently under investigation. Once a procedure is set up to deal with the sector integrals numerically for general kinematics, a numerical approach for multi-leg and multi-loop processes relevant at present and future high energy experiments will be feasible. In the meantime, nonetheless, the algorithm serves as an independent check for analytical results of multi-loop integrals.

Acknowledgements

G.H. would like to thank V.A. Smirnov for a stimulating exchange of results.

References

- [1] T. Binoth, G. Heinrich, Nucl. Phys. B **585** (2000) 741 [arXiv:hep-ph/0004013].

- [2] V.A. Smirnov, Phys. Lett. **B460**, 397 (1999) [hep-ph/9905323].
- [3] J.B. Tausk, Phys. Lett. **B469**, 225 (1999) [hep-ph/9909506].
- [4] V. A. Smirnov, Phys. Lett. B **491** (2000) 130 [arXiv:hep-ph/0007032].
- [5] T. Gehrmann and E. Remiddi, Nucl. Phys. B **601** (2001) 248 [arXiv:hep-ph/0008287].
- [6] V. A. Smirnov, Phys. Lett. B **500** (2001) 330 [arXiv:hep-ph/0011056].
- [7] T. Gehrmann and E. Remiddi, Nucl. Phys. B **601** (2001) 287 [arXiv:hep-ph/0101124].
- [8] Z. Bern, L. J. Dixon and A. Ghinculov, Phys. Rev. D **63** (2001) 053007 [arXiv:hep-ph/0010075]; C. Anastasiou, E. W. N. Glover, C. Oleari and M. E. Tejeda-Yeomans, Nucl. Phys. B **601** (2001) 318 [arXiv:hep-ph/0010212]; C. Anastasiou, E. W. N. Glover, C. Oleari and M. E. Tejeda-Yeomans, Nucl. Phys. B **601** (2001) 341 [arXiv:hep-ph/0011094]; C. Anastasiou, E. W. N. Glover, C. Oleari and M. E. Tejeda-Yeomans, Nucl. Phys. B **605** (2001) 486 [arXiv:hep-ph/0101304]; E. W. N. Glover, C. Oleari and M. E. Tejeda-Yeomans, Nucl. Phys. B **605** (2001) 467 [arXiv:hep-ph/0102201]; Z. Bern, L. J. Dixon and D. A. Kosower, JHEP **0001** (2000) 027 [arXiv:hep-ph/0001001]; Z. Bern, A. De Freitas and L. Dixon, JHEP **0203** (2002) 018 [arXiv:hep-ph/0201161]; Z. Bern, A. De Freitas and L. J. Dixon, JHEP **0109** (2001) 037 [arXiv:hep-ph/0109078]; Z. Bern, A. De Freitas, L. J. Dixon, A. Ghinculov and H. L. Wong, JHEP **0111** (2001) 031 [arXiv:hep-ph/0109079]; T. Binoth, E. W. N. Glover, P. Marquard and J. J. van der Bij, JHEP **0205** (2002) 060 [arXiv:hep-ph/0202266]; C. Anastasiou, E. W. N. Glover and M. E. Tejeda-Yeomans, Nucl. Phys. B **629** (2002) 255 [arXiv:hep-ph/0201274]; E. W. Glover and M. E. Tejeda-Yeomans, arXiv:hep-ph/0304169.
- [9] L. W. Garland, T. Gehrmann, E. W. N. Glover, A. Koukoutsakis and E. Remiddi, Nucl. Phys. B **627** (2002) 107 [arXiv:hep-ph/0112081]; L. W. Garland, T. Gehrmann, E. W. N. Glover, A. Koukoutsakis and E. Remiddi, Nucl. Phys. B **642** (2002) 227 [arXiv:hep-ph/0206067]; S. Moch, P. Uwer and S. Weinzierl, Phys. Rev. D **66** (2002) 114001 [arXiv:hep-ph/0207043].
- [10] A. Ferroglia, M. Passera, G. Passarino and S. Uccirati, Nucl. Phys. B **650** (2003) 162 [arXiv:hep-ph/0209219].
- [11] T. Binoth, G. Heinrich and N. Kauer, Nucl. Phys. B **654** (2003) 277 [arXiv:hep-ph/0210023].

- [12] F. V. Tkachov, Nucl. Instrum. Meth. A **389** (1997) 309 [arXiv:hep-ph/9609429];
F. V. Tkachov, Phys. Lett. B **412** (1997) 350 [arXiv:hep-ph/9703424].
- [13] A. Ghinculov and Y. P. Yao, Phys. Rev. D **63** (2001) 054510
[arXiv:hep-ph/0006314].
- [14] G. Passarino, Nucl. Phys. B **619** (2001) 257 [arXiv:hep-ph/0108252];
G. Passarino and S. Uccirati, Nucl. Phys. B **629** (2002) 97
[arXiv:hep-ph/0112004].
- [15] V. A. Smirnov, *Applied Asymptotic Expansions in Momenta and Masses*,
Springer, Berlin, Heidelberg 2002.
- [16] K. Hepp, Commun. Math. Phys. **2** (1966) 301.
- [17] M. Roth and A. Denner, Nucl. Phys. B **479** (1996) 495 [arXiv:hep-ph/9605420].
- [18] A. Denner, M. Melles and S. Pozzorini, arXiv:hep-ph/0301241.
- [19] G. Heinrich, Nucl. Phys. Proc. Suppl. **116** (2003) 368 [arXiv:hep-ph/0211144].
- [20] V. A. Smirnov, Nucl. Phys. Proc. Suppl. **116** (2003) [arXiv:hep-ph/0209295].
- [21] V. A. Smirnov, hep-ph/0305142.
- [22] N. Nakanishi, Graph Theory and Feynman Integrals, Gordon and Breach, New
York 1971.
- [23] O. I. Zavialov, *Renormalized Quantum Field Theory*, Kluwer 1990. Translation
of a Russian book published in 1979.
- [24] C. Itzykson, J. B. Zuber, *Quantum Field Theory*, World Scientific 1993.
- [25] A. I. Davydychev, Phys. Lett. B **263** (1991) 107.
- [26] O. V. Tarasov, Phys. Rev. **D54** 6479 (1996).
- [27] K. G. Chetyrkin and F. V. Tkachov, Nucl. Phys. B **192** (1981) 159, and private
communication.
- [28] M. Steinhauser, Phys. Rept. **364** (2002) 247 [arXiv:hep-ph/0201075].
- [29] S. Laporta, Phys. Lett. B **549** (2002) 115 [arXiv:hep-ph/0210336].
- [30] S. Kawabata, Comp. Phys. Commun. **88** (1995) 309.